Supplemental information

ALKB-1-Dependent tRNA Methylation is Required for Efficient Paternal Mitochondrial Elimination

Zhenhuan Luo [1, 2, 3, #], Yimin Li [4, 5, #], Chenyang He [2, 3, 5], Dan Wu [2, 3, 5], Wenyu Dai [2, 3, 5], Liubing Hu [5], Jing Yang [3, 5], Brian L Harry [6], Zhenyu Ju [7], Nektarios Tavernarakis [8], Hao Wang [2], Qin-Li Wan [4, 5, *] & Qinghua Zhou [2, 3, 9, 10, *]

[1] Department of Cardiology, The First Affiliated Hospital, Jinan University, Guangzhou, Guangdong, China, 510632.

[2] Shantou Clinical Medical College of Jinan University (Shantou Central Hospital), Jinan University, Shantou, Guangdong, China, 515041.

[3] College of Life Science and Technology, Jinan University, Guangzhou, Guangdong, China, 510632.

[4] Department of pathogen biology, school of medicine, Jinan University, Guangzhou, Guangdong, China, 510632.

[5] The Biomedical Translational Research Institute, Faculty of Medical Science, Jinan University, Guangzhou, Guangdong, China, 510632.

[6] Department of Pathology, Michigan Medicine, University of Michigan, Ann Arbor, USA, 48109.

[7] Key Laboratory of Regenerative Medicine of Ministry of Education, Institute of Aging and Regeneration Medicine, Jinan University, Guangzhou, Guangdong, China, 510632.

[8] Institute of Molecular Biology and Biotechnology, Foundation of Research and Technology-Hellas Department of Basic Sciences, School of Medicine, University of Crete Heraklion, Crete, Greece, GR-70013.

[9] State Key Laboratory of Bioactive Molecules and Druggability Assessment, Guangdong Basic Research Center of Excellence for Natural Bioactive Molecules and Discovery of Innovative Drugs, Jinan University, Guangzhou, Guangdong, China, 510632.

[10] National Engineering Research Center of Genetic Medicine, Guangzhou, Guangdong, China, 510632.

[#] These authors contributed equally: Zhenhuan Luo, Yimin Li.

[*] e-mail: gene@email.jnu.edu.cn, wanqinli@hotmail.com.

Contents

Supplementary Figure 1. Characterization of the role of ALKB-1 in PME, through RNAi screen

Supplementary Figure 2. ALKB-1 localizes diffusely to multiple compartments including mitochondria

Supplementary Figure 3. ALKB-1 enzymatic activity is essential for proper PME

Supplementary Figure 4. ALKB-1 inactivation underlies PME defects via mitochondrial and mtDNA proliferation in sperm

Supplementary Figure 5. ALKB-1 alters translational homeostasis through tRNA m^1A demethylation in *C. elegans*

Supplementary Figure 6. ALKB-1 deficiency disrupts mitochondrial protein homeostasis

Supplementary Figure 7. ALKB-1 inactivation triggers UPR^{mt} in *C. elegans*

Supplementary Figure 8. ALKB-1 inactivation results in impaired ETC and elevated mtROS

Supplementary Figure 9. Male sperm development proceeds normally in ALKB-1-deficient worms

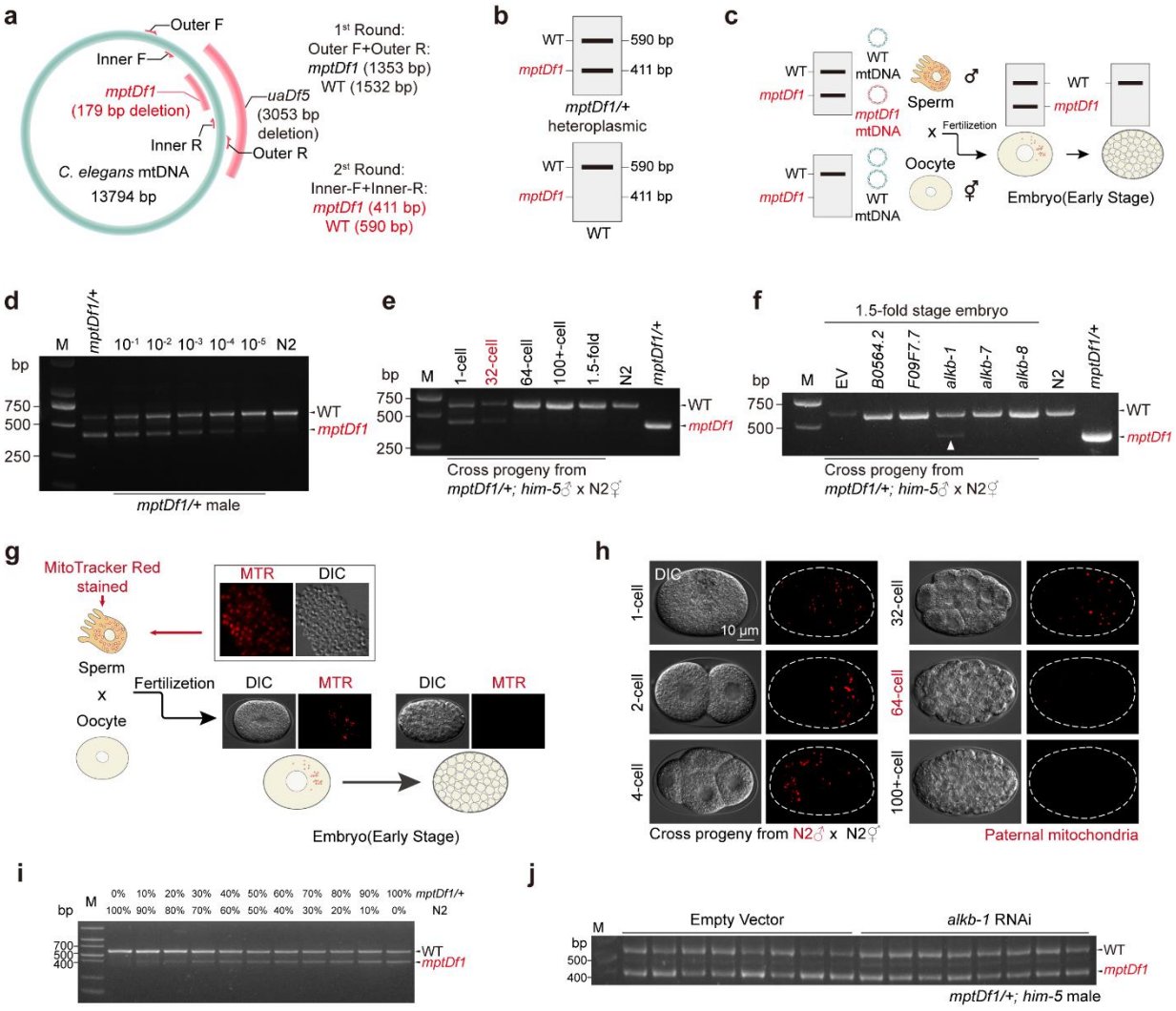
Supplementary Figure 10. UPR^{mt} activation alone is insufficient to cause PME defects

Supplementary Figure 11. Knockdown of *alkb-1* affects autophagy induction in *C. elegans*

Supplementary Figure 12. Epistasis analysis places ALKB-1 upstream of CPS-6 and LGG-1 in the PME process

Supplementary Table 1. The primers used in RT-qPCR

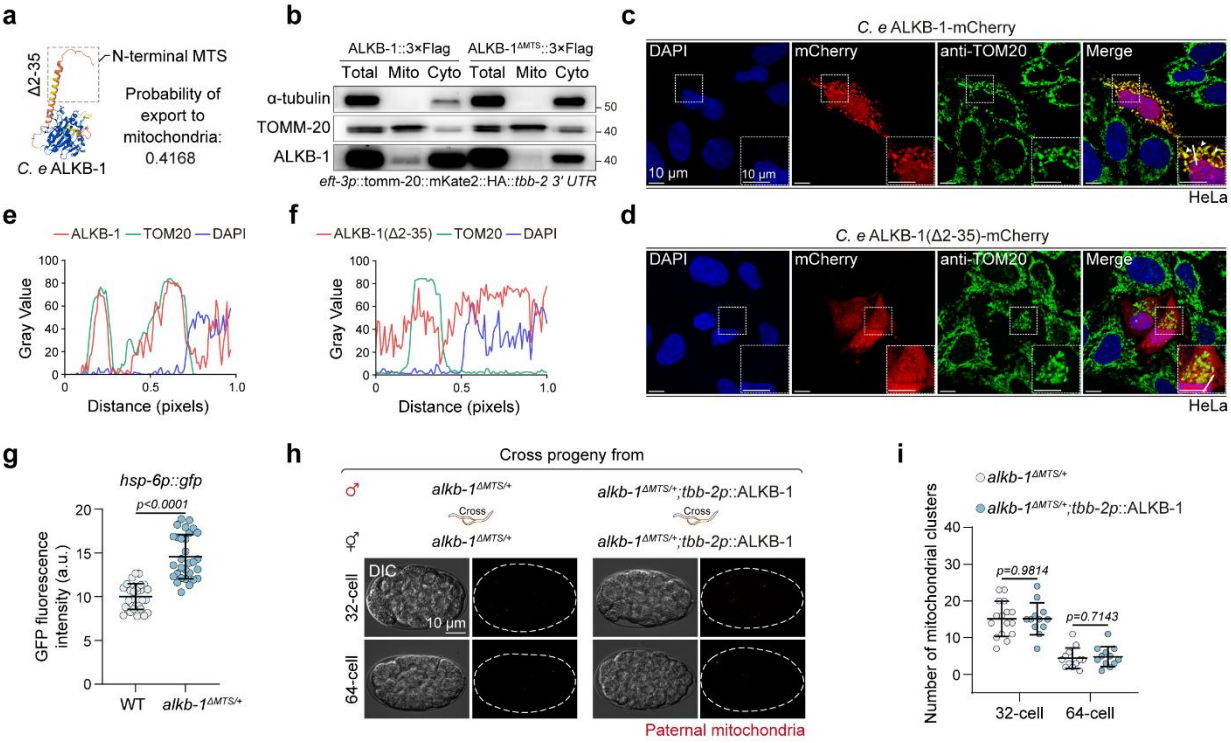
Supplementary Table 2. The primers used in biotin-labeled Northern blot



Supplementary Figure 1. Characterization of the role of ALKB-1 in PME, through RNAi screen

a Schematic diagram of wild-type mtDNA and mutant mtDNA in *C. elegans*, with red marks indicating the deleted segments of *uaDf5* and *mptDf1*, detected specifically using Outer F/R + Inner F/R primers for *mptDf1* mtDNA. **b** Schematic diagram of specific bands for the nested PCR detection of wild-type and *mptDf1* mtDNA. **c** Schematic diagram of the nested PCR method used to detect paternal *mptDf1* mtDNA in cross-fertilized embryos. **d** PCR amplification products of *mptDf1* mtDNA using Outer F/R and Inner F/R primers, with gradient dilution (10^{-1} - 10^{-5}) of *mptDf1*/+ male samples. **e** *mptDf1* mtDNA-based PCR assays

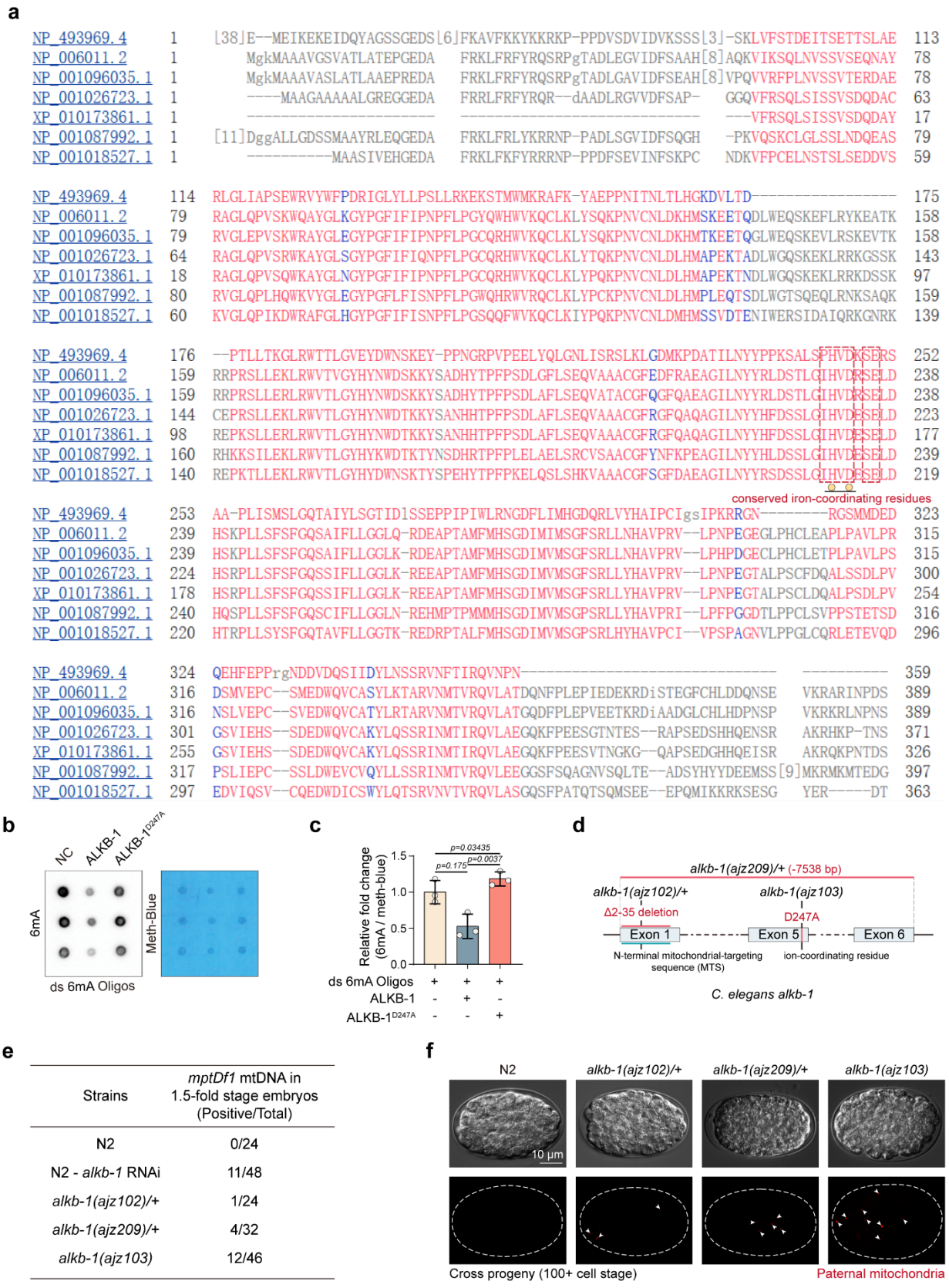
used to monitor the persistence of paternal *mptDf1* mtDNA in several stage cross-fertilized embryos from mating of *mptDf1/+; him-5 (e1467)* males with wild-type N2 hermaphrodites. **f** *mptDf1* mtDNA-based PCR assays used to monitor the persistence of paternal *mptDf1* mtDNA in 1.5-fold stage cross-fertilized embryos from mating of *mptDf1/+; him-5 (e1467)* males with N2 hermaphrodites under different RNAi conditions: empty vector (EV), *B0564.2*, *F09F7.7*, *alkb-1*, *alkb-7*, or *alkb-8*. **g** Schematic outline of MTR fluorescence staining method for tracking mitochondrial distribution. **h** Representative DIC and MTR-stained paternal mitochondrial images of the 1-, 2-, 4-, 32-, 64-, and 100+-cell stage cross-fertilized embryos from mating of MTR-stained N2 males with hermaphrodites, with scale bars of 10 μm. **i** PCR amplification products of *mptDf1* mtDNA were obtained using outer and inner F/R primers from samples containing mixed populations of *mptDf1/+* and wild-type N2 males in defined ratios ranging from 0% to 100%. Heteroplasmy levels were quantified by grayscale scanning of the wild-type and *mptDf1*-specific bands. **j** Comparison of *mptDf1* heteroplasmy levels in empty vector versus *alkb-1* RNAi males, as determined by nested PCR with outer and inner F/R primers.



Supplementary Figure 2. ALKB-1 localizes diffusely to multiple compartments including mitochondria

a Schematic diagram showing the protein structure and regions of the predicted mitochondrial targeting peptide sequence (MTS) of *C. elegans* ALKB-1. **b** Western blot analyses of transgenic worms expressing ALKB-1::3×FLAG or ALKB-1$^{\Delta MTS}$::3×FLAG, with TOMM-20::mKate2::HA, after fractionation into total lysate (Total), cytoplasm supernatant (Cyto), and mitochondrial pellet (Mito). The anti-α-tubulin immunoblot served as a cytosolic maker, the anti-HA immunoblot served as a mitochondrial maker (TOMM-20::mKate2::HA), and ALKB-1::3×FLAG was detected by an anti-FLAG antibody. n = 3 biological repeats. **c, d** Representative immunofluorescence images showing DAPI, ALKB-1::mCherry, and TOM20 in HeLa cells transfected with pcDNA3.1(+)-pCMV-ALKB-1-mCherry **(c)** and pcDNA3.1(+)-pCMV-ALKB-1(Δ2-35)-mCherry **(d)** plasmid, with scale bars of 10 μm. The experiment was performed three times with similar results. **e, f** The fluorescence intensity of mCherry, GFP,

and DAPI signals in a cross-section of several fluorescence puncta from **(c)** and **(d)**, as indicated by the white diagonal line in the merge panel. **g** Quantification of fluorescence intensity for the *hsp-6p::gfp* reporter in wild-type and *alkb-1*$^{\Delta MTS/+}$ hermaphrodites. (n = 30 per group). The experiment was performed twice with similar results. **h** Representative DIC and MTR-stained paternal mitochondrial images of the 32- and 64-cell stage embryos from cross-fertilization of the indicated strain males (stained by MTR) with hermaphrodites, with scale bars of 10 μm. **i** Quantification of the number of MTR-labeled mitochondrial clusters in **(h)**. n = 16 (*alkb-1*^{D247A}, 32-cell), n = 12 (*alkb-1*^{D247A}, 64-cell, and *alkb-1*$^{\Delta MTS/+}$, 32- and 64-cell). Embryos were derived from 3 – 5 independent biological crosses per condition. The experiment was performed twice with similar results. Data were presented as mean ± SD. *p*-values were determined by unpaired two-tailed t-test **(g)** and **(i)**. Source data are provided as a Source Data file.

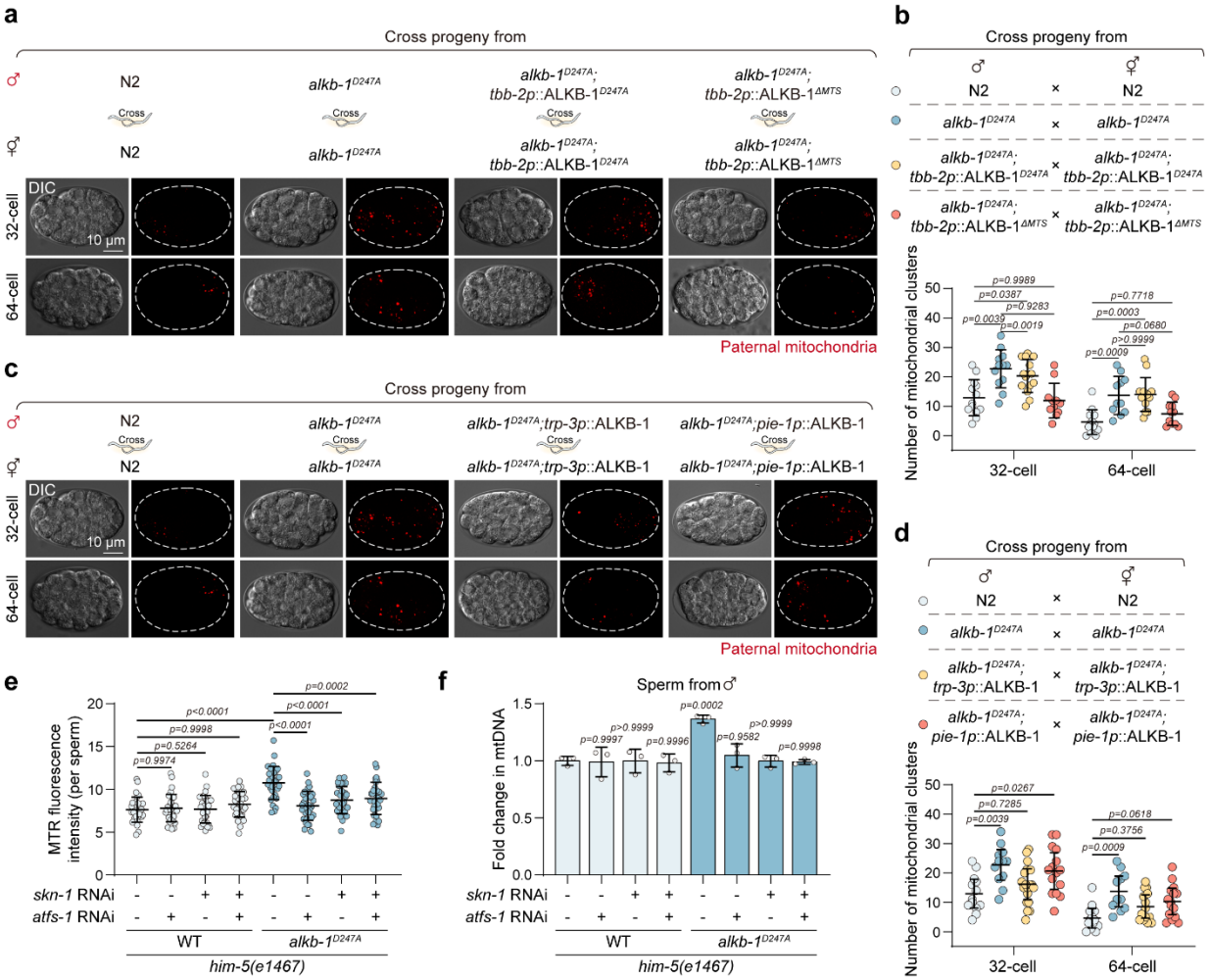


Strains	*mptDf1* mtDNA in 1.5-fold stage embryos (Positive/Total)
N2	0/24
N2 - *alkb-1* RNAi	11/48
alkb-1(ajz102)/+	1/24
alkb-1(ajz209)/+	4/32
alkb-1(ajz103)	12/46

Supplementary Figure 3 ALKB-1 enzymatic activity is essential for proper PME

a Multiple sequence alignment of ALKB-1 and ALKBH1 homologs reveals conserved residues

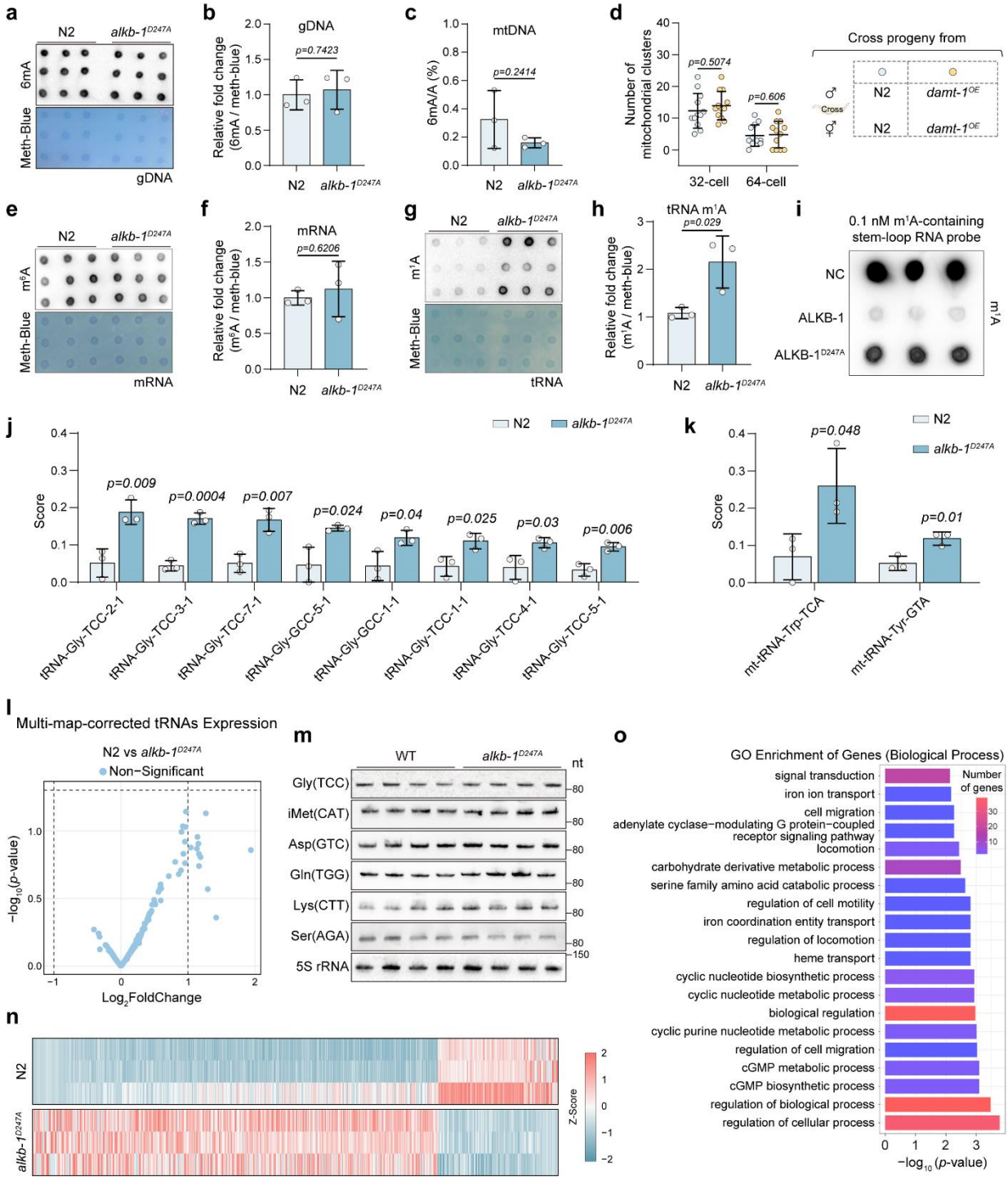
and domains**. b, c** Representative 6mA dot blot analyses **(b)** and quantification **(c)** for ds 6mA Oligos treated with vehicle (NC), wild-type ALKB-1, or the catalytically inactive mutant ALKB-1 (ALKB-1^{D247A}). Methylene blue (Meth-Blue) was used to detect oligos loading. n = 3 biological repeats. **d** Schematic diagram showing the deletion fragments or mutation sites of ALKB-1 mutants, including *alkb-1 (ajz209)*/+, *alkb-1 (ajz102)*/+, and *alkb-1 (ajz103)*. **e** *mptDf1* mtDNA-based PCR assays used to monitor persistence of paternal *mptDf1* mtDNA in cross-fertilized 1.5-fold stage embryos from the indicated crosses. **f** Representative DIC and MTR-stained paternal mitochondrial images of 100+-cell stage embryos from cross-fertilization of the indicated strain males (stained by MTR) with hermaphrodites. The puncta marked with white arrowheads represented the MTR-stained mitochondrial from sperm, with scale bars of 10 μm. The experiment was performed three times with similar results. Data were represented as mean ± SD; *p*-values were determined by one-way ANOVA with Tukey's multiple comparisons test **(c)**. Source data are provided as a Source Data file.



Supplementary Figure 4. ALKB-1 inactivation underlies PME defects via mitochondrial and mtDNA proliferation in sperm

a, c Representative DIC and MTR-stained paternal mitochondrial images of the 32- and 64-cell stage embryos from cross-fertilization of the indicated strain males (stained by MTR) with hermaphrodites, with scale bars of 10 μm. N2 and *alkb-1*^{D247A} mutant images are shared between these panels. **b, d** Quantification of the number of MTR-labeled mitochondrial clusters in **(a)** and **(c)**. Data for the N2 and *alkb-1*^{D247A} mutant are shared between these panels. n = 13 (N2, 32- and 64-cell), n = 12 (*alkb-1*^{D247A}, 32-cell), n = 11 (*alkb-1*^{D247A}, 64-cell), n = 15 (*alkb-1*^{D247A}*; tbb-2p::*ALKB-1^{D247A}, 32-cell), n = 13 (*alkb-1*^{D247A}*; tbb-2p::*ALKB-1^{D247A}, 64-cell), n = 11 (*alkb-1*^{D247A}*; tbb-2p::*ALKB-1$^{\Delta MTS}$, 32- and 64-cell), n = 20 (*alkb-1*^{D247A}*; trp-*

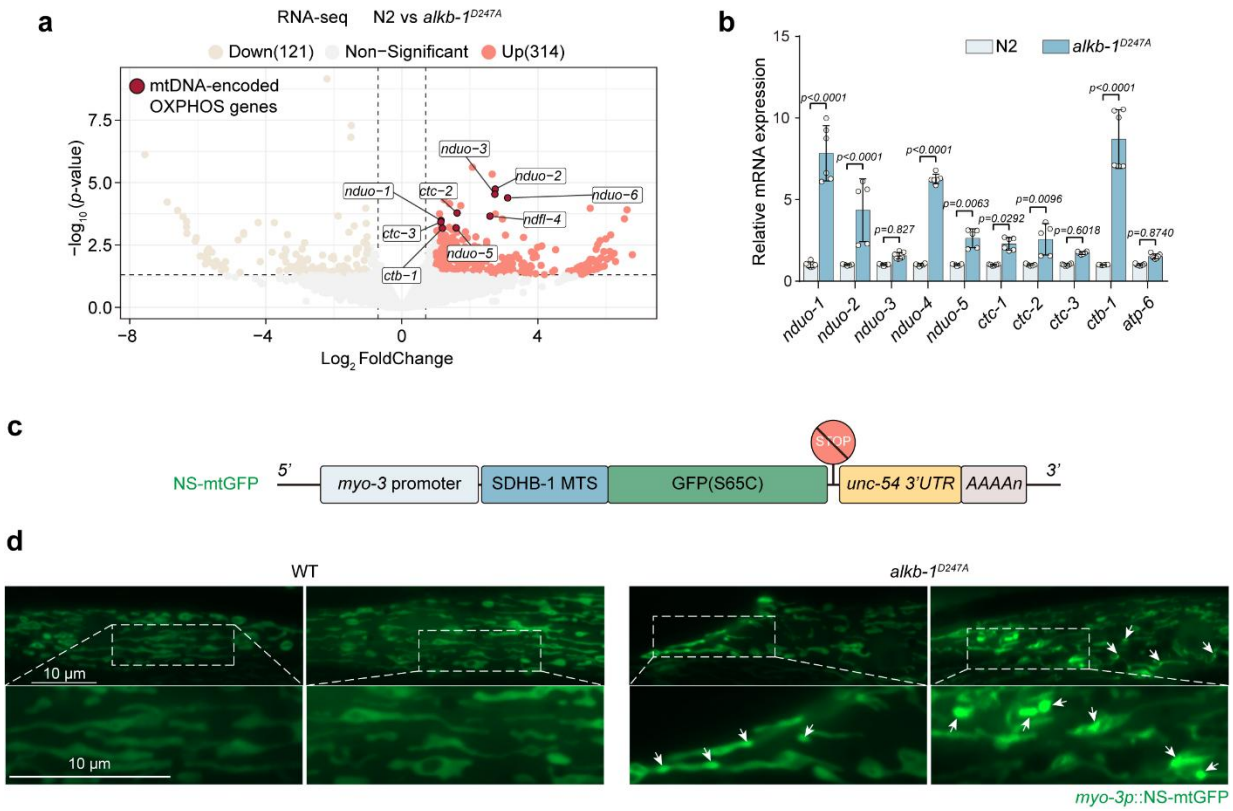
*3p::*ALKB-1, 32-cell), n = 14 (*alkb-1*^{D247A}*; trp-3p::*ALKB-1, 64-cell), n = 15 (*alkb-1*^{D247A}*; pie-1p::*ALKB-1, 32- and 64-cell). Embryos were derived from 3 – 5 independent biological crosses per condition. The experiment was performed twice with similar results. **e** Quantification of the fluorescence intensity of MTR in sperm dissected from the *him-5 (e1467)* and *alkb-1*^{D247A}*; him-5 (e1467)* males exposed to control RNAi, *atfs-1* RNAi, *skn-1* RNAi, or *atfs-1* and *skn-1* double RNAi, stained with MTR (n = 30 per group). **f** Quantification of the level of total mtDNA in the sperm dissected from the *him-5 (e1467)* and *alkb-1*^{D247A}*; him-5 (e1467)* males treated with control RNAi, *atfs-1* RNAi, *skn-1* RNAi, or *atfs-1* and *skn-1* double RNAi (n= 3 per group). Data were presented as mean ± SD. *p*-values were determined by Ordinary one-way ANOVA with Tukey's multiple comparisons test **(b)**, **(d)**, **(e)**and **(f)**. Source data are provided as a Source Data file.



Supplementary Figure 5. ALKB-1 alters translational homeostasis through tRNA m¹A demethylation in *C. elegans*

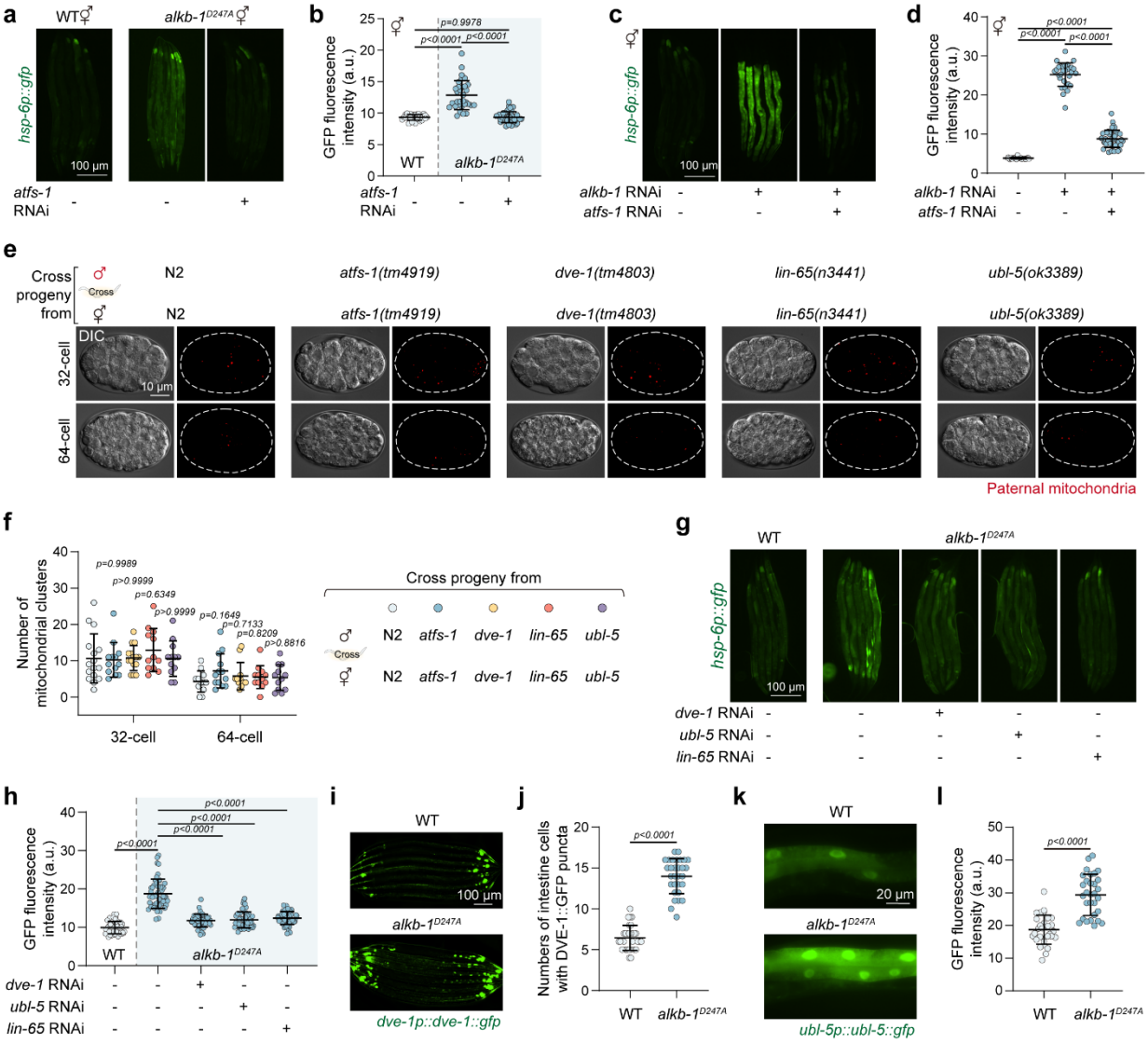
a, b Representative 6mA dot blot analyses **(a)** and quantification **(b)** of gDNA from N2 and *alkb-1*^{D247A} worms (n = 3). Methylene blue (Meth-Blue) was used to detect gDNA loading. **c**

Quantification of mtDNA 6mA modifications in N2 and *alkb-1*^{D247A} worms using LC-MS. **d** Quantification of the number of MTR-labeled mitochondrial clusters in the 32- and 64-cell stage embryos from cross-fertilization of the indicated strain males (stained by MTR) with hermaphrodites (n = 12 per group). Embryos were derived from 3 – 5 independent biological crosses per condition. The experiment was performed twice with similar results. **e, f** Representative m^{6}A dot blot analyses **(e)** and quantification **(f)** of mRNA from N2 and *alkb-1*^{D247A} worms (n = 3). Meth-Blue was used to detect mRNA loading. **g, h** Representative m^{1}A dot blot analyses **(g)** and quantification **(h)** of tRNA from N2 and *alkb-1*^{D247A} worms (n = 3). Meth-Blue was used to detect tRNA loading and m^{1}A antibody (ab208196, abCam) was used. **i** Representative m^{1}A dot blot analyses for stem-loop structured m^{1}A tRNA probes treated with vehicle (NC), wild-type ALKB-1, or the catalytically inactive mutant ALKB-1 (ALKB-1^{D247A}). n = 3 biological repeats. **j, k** Quantification of the tRNAs with the significant increased m^{1}A modification in N2 and *alkb-1*^{D247A} worms through tRNA m^{1}A seq analysis, including cytosolic tRNA (Gly) **(j)** and two mitochondrial tRNAs **(k)**. **l** Volcano plot of all identified tRNAs abundance in *alkb-1*^{D247A} worms compared with N2 worms. **m** Biotin-labeled Northern blot results showing tRNA levels in Gly-TCC, iMet-CAT, Asp-GTC, Gln-TGG, Lys-CTT, and Ser-AGA. 5S rRNA served as loading control. **n** Heatmap showing cluster analysis of the genes with differential translation efficiency (TE) between N2 and *alkb-1*^{D247A} worms as determined by RNC-seq. **o** GO-BP term analysis of the genes with increased TE in the *alkb-1*^{D247A} worms compared to N2. Data were represented as mean ± SD. *p*-values were determined by unpaired two-tailed t-test (**b**), **(c)**, **(d)**, **(f)**, **(h)**, **(j)** and **(k)**. Source data are provided as a Source Data file.



Supplementary Figure 6. ALKB-1 deficiency disrupts mitochondrial protein homeostasis

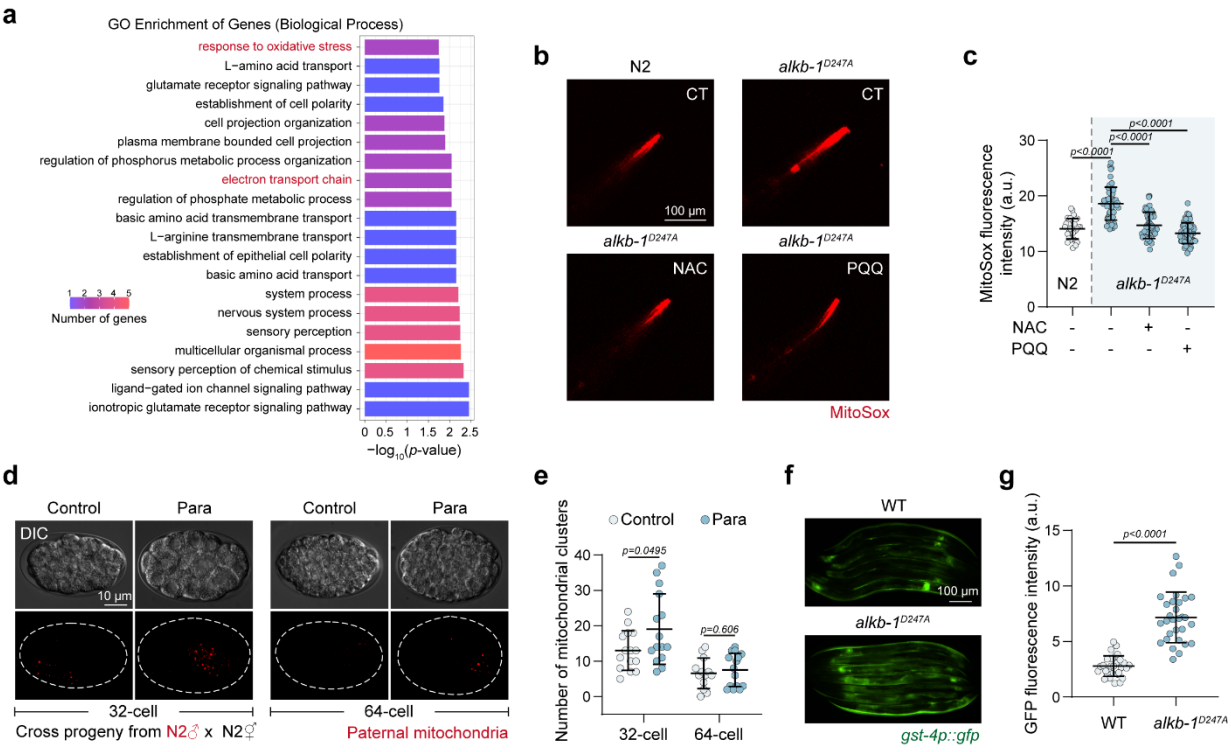
a Volcano plot depicting the differentially expressed genes in *alkb-1*^{D247A} worms compared with N2 from RNA-seq analysis, with OXPHOS genes upregulated in *alkb-1*^{D247A} highlighted. **b** RT-qPCR analysis of the mtDNA-encoded OXPHOS genes in WT and *alkb-1*^{D247A} worms (n ≥ 5 biologically independent samples). **c** Schematic diagram of the NS-mtGFP transgenic vector. **d** Representative images of the NS-mtGFP puncta in the bady wall muscle cells in wild-type and *alkb-1*^{D247A} animals. **Bottom**: magnified images of the white dashed-line square in the Top panel, with scale bars of 10 μm. White arrowheads indicate NS-mtGFP puncta accumulated in mitochondria. The experiment was performed three times with similar results. Data were represented as mean ± SD. *p*-values were determined by unpaired two-tailed t-test **(b)**. Source data are provided as a Source Data file.



Supplementary Figure 7. ALKB-1 inactivation triggers UPR^{mt} in *C. elegans*

a, b Representative fluorescence images **(a)** and quantification **(b)** of the *hsp-6p::gfp* reporter in wild-type and *alkb-1*^{D247A} hermaphrodites, with wild-type hermaphrodites were fed with control RNAi (n = 30) and *alkb-1*^{D247A} worms were fed with control (n = 32) or *atfs-1* RNAi (n = 40), with scale bars of 100 μm. The experiment was performed three times with similar results. **c, d** Representative fluorescence images **(c)** and quantification **(d)** the *hsp-6p::gfp* reporter in wild-type animals fed with control RNAi (n = 40), *alkb-1* RNAi (n = 31), or a combination of *alkb-1* and *atfs-1* RNAi (n = 40), with scale bars of 100 μm. The experiment

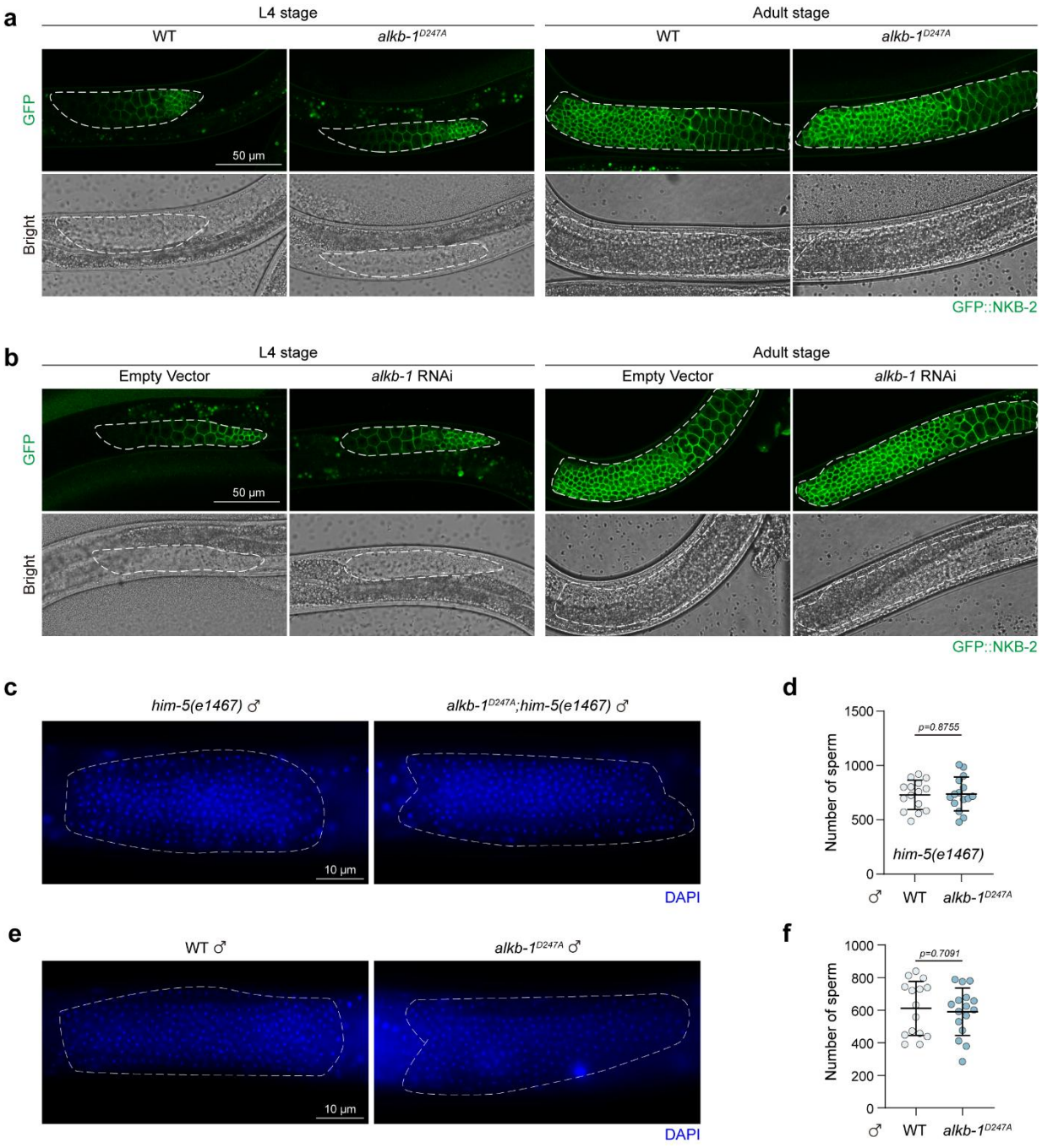
was performed three times with similar results. **e** Representative DIC and MTR-stained paternal mitochondrial images of the 32- and 64-cell stage embryos from cross-fertilization of the indicated strain males (stained by MTR) with hermaphrodites, with scale bars of 10 μm. **f** Quantification of the number of MTR-labeled mitochondrial clusters in **(e)**. n = 16 (N2, 32-cell), n = 12 (N2, 64-cell), n = 13 (*atfs-1*, 32- and 64-cell), n = 15 (*dve-1*, 32-cell), n = 12 (*dve-1*, 64-cell), n = 12 (*lin-65* and *ubl-5*, 32- and 64-cell). **g, h** Representative fluorescence images **(g)** and quantification **(h)** of the *hsp-6p::gfp* reporter in wild-type and *alkb-1*^{D247A} animals, the wild-type worms were fed with control RNAi, and the *alkb-1*^{D247A} worms were fed with control, *dve-1* RNAi, *ubl-5* RNAi, or *lin-65* RNAi (n = 50 per group), with scale bars of 100 μm. **i** Representative fluorescence images of the *dve-1p::dve-1::gfp* reporter in wild-type and *alkb-1*^{D247A} animals (n = 30 per group), with scale bars of 100 μm. **j** Quantification of the number of intestine cells with DVE-1::GFP puncta in posterior region per animal (n = 30 per group), as depicted in **(i)**. **k, l** Representative fluorescence images **(k)** and quantification **(l)** of the *ubl-5p::ubl-5::gfp* reporter in wild-type and *alkb-1*^{D247A} animals, with scale bars of 20 μm. In **(f)**, embryos were derived from 3 – 5 independent biological crosses per condition. The experiment was performed twice with similar results. Data were represented as mean ± SD. *p*-values were determined by Ordinary one-way ANOVA with Tukey's multiple comparisons test **(b)**, **(d)**, **(f)** and **(h)** and unpaired two-tailed t-test **(j)** and **(l)**. Source data are provided as a Source Data file.



Supplementary Figure 8. ALKB-1 inactivation results in impaired ETC and elevated mtROS

a GO-BP analysis of genes exhibiting differential translation initiation efficiency in the *alkb-1*^{D247A} worms compared to N2. **b, c** Representative images **(b)** and quantification **(c)** of fluorescence in the head region of N2 (n = 31), *alkb-1*^{D247A} (n = 58), and *alkb-1*^{D247A} worms treated with 5 mM NAC (n = 50) or 1 mM PQQ (n = 60), as stained with mtSOX, with scale bars of 100 µm. **d** Representative DIC and MTR-labeled images of mitochondria in 32- and 64-cell stage embryos from cross-fertilization of the N2 males (stained by MTR) with hermaphrodites under the indicated treatment, with scale bars of 10 µm. **e** Quantification of the number of MTR-labeled mitochondrial clusters depicted in **(d)**. n = 15 (N2 treated with control, 32-cell, and N2 treated with Paraque, 32- and 64-cell), n = 13 (N2 treated with control, 64-cell). Embryos were derived from 3 – 5 independent biological crosses per condition. The experiment was performed twice with similar results. **f, g** Representative images **(f)** and

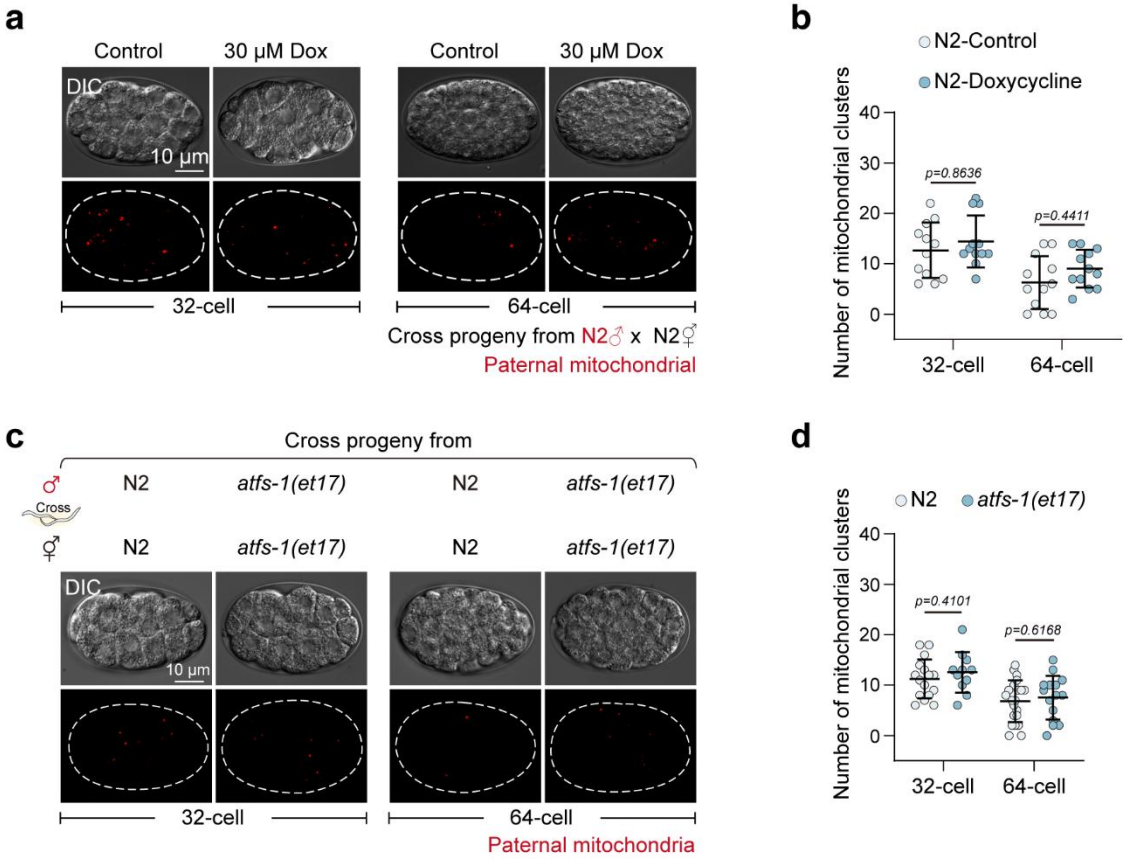
quantification **(g)** of *gst-4p::gfp* fluorescence in wild-type and *alkb-1*^{D247A} worms (n = 30 per group). Scale bars, 100 μm. Data were represented as mean ± SD. *p*-values were determined by Ordinary one-way ANOVA with Tukey's multiple comparisons test **(c)** and unpaired two-tailed t-test **(e)** and **(g)**. Source data are provided as a Source Data file.



Supplementary Figure 9. Male sperm development proceeds normally in ALKB-1-deficient worms

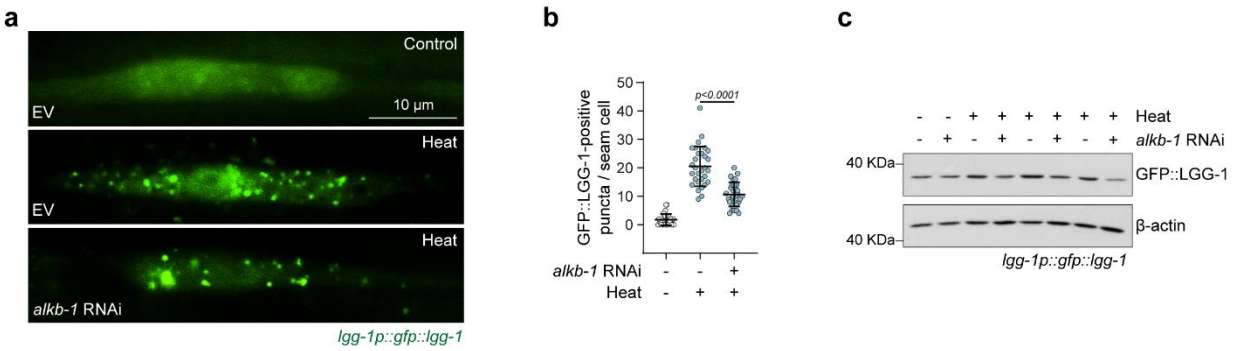
a, b Representative fluorescence images of the GFP::NKB-2 reporter in the germline and seminal vesicles of young adult and adult males. Images compare wild-type and *alkb-1*^{D247A} mutants **(a)**, and wild-type males fed control vs *alkb-1* RNAi **(b)**. The experiment was performed three times with similar results. Scale bars, 50 µm. **c-f** Representative images **(c, e)**

and quantification **(d, f)** of DAPI-stained spermatids in the seminal vesicle of *him-5 (e1467)* (n = 15) vs *alkb-1*^{D247A}*; him-5 (e1467)* (n = 15) males **(c, d)**, and N2 (n = 15) vs *alkb-1*^{D247A} (n = 16) males **(e, f)**, with scale bars of 10 μm. Data were represented as mean ± SD. *p*-values were determined by unpaired two-tailed t-test **(d)** and **(f)**. Source data are provided as a Source Data file.



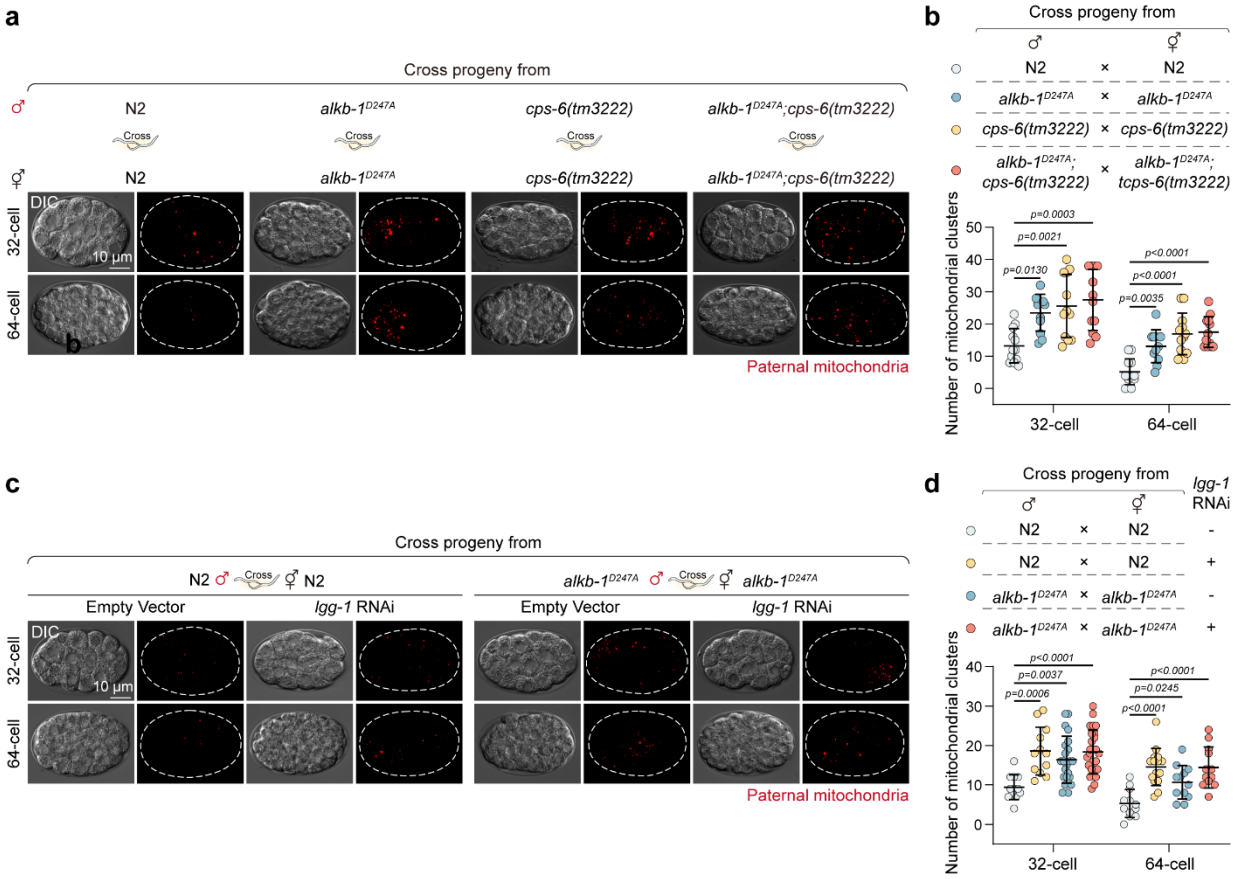
Supplementary Figure 10. UPR^{mt} activation alone is insufficient to cause PME defects

a, c Representative DIC and MTR-stained paternal mitochondrial images of the 32- and 64-cell stage embryos from cross-fertilization of the indicated strain males (stained by MTR) with hermaphrodites, with scale bars of 10 μm. **b, d** Quantification of the number of MTR-labeled mitochondrial clusters in the 32- and 64-cell stage embryos from cross-fertilization of the indicated strain males (stained by MTR) with hermaphrodites in **(a)** and **(c)**, respectively. In **(b)**, n = 12 per group. In **(d)**, n = 16 (N2, 32-cell), n = 21 (N2, 64-cell), n = 11 (*atfs-1(et17)*, 32-cell), n = 15 (*atfs-1(et17)*, 64-cell). Embryos were derived from 3 – 5 independent biological crosses per condition. The experiment was performed twice with similar results. Data were presented as mean ± SD. *p*-values were determined by one-way analysis of variance (ANOVA) **(b)** and **(d)**. Source data are provided as a Source Data file.



Supplementary Figure 11. Knockdown of *alkb-1* affects autophagy induction in *C. elegans*

a, b Representative images **(a)** and quantification **(b)** of the GFP::LGG-1 puncta in the hypodermal seam cells of wild-type worms fed with control or *alkb-1* RNAi, with or without heat treatment at 35 °C for 1.5 hours (n = 30 per group). The experiment was performed three times with similar results. **c** Protein levels of GFP::LGG-1 in wild-type worms fed with control or *alkb-1* RNAi, with or without heat treatment. n = 3 biological repeats. Data were represented as mean ± SD. *p*-values were determined by Ordinary one-way ANOVA with Tukey's multiple comparisons test **(b)**. Source data are provided as a Source Data file.



Supplementary Figure 12. Epistasis analysis places ALKB-1 upstream of CPS-6 and LGG-1 in the PME process

a, c Representative DIC and MTR-stained paternal mitochondrial images of the 32- and 64-cell stage embryos from cross-fertilization of the indicated strain males (stained by MTR) with hermaphrodites, with scale bars of 10 μm. **b, d** Quantification of the number of MTR-labeled mitochondrial clusters in the 32- and 64-cell stage embryos from cross-fertilization of the indicated strain males (stained by MTR) with hermaphrodites in **(a)** and **(c)**, respectively. In **(b)**, n = 12 for all groups except *alkb-1*^{D247A} 64-cell (n = 11). In **(d)**, n = 12 (N2 - EV, 32- and 64-cell), n = 12 (N2 - *lgg-1* RNAi, 32-cell), n = 15 (N2 - *lgg-1* RNAi, 64-cell), n = 22 (*alkb-1*^{D247A} - EV, 32-cell), n = 12 (*alkb-1*^{D247A} - EV, 64-cell), n = 26 (*alkb-1*^{D247A} - *lgg-1* RNAi, 32-cell), n = 12 (*alkb-1*^{D247A} - *lgg-1* RNAi, 64-cell). Embryos were derived from 3 – 5 independent biological crosses per condition. The experiment was performed twice with similar results.

Data were presented as mean ± SD. *p*-values were determined by Ordinary one-way ANOVA with Tukey's multiple comparisons test **(b)** and **(d)**. Source data are provided as a Source Data file.

Supplementary Table 1. The primers used in RT-qPCR

Gene		Primer sequences (5'-3')
cdc-42	Forward	CTGCTGGACAGGAAGATTACG
	Reverse	CTCGGACATTCTCGAATGAAG
alkb-1	Forward	CGCTTGCTGAGAGATTAGGTCT
	Reverse	ACATCCTTTCCGTGAAGCGT
nduo-1	Forward	GGCCATCCGTGCTAGAAGAC
	Reverse	AAATGGCGCCCGGTTAAGTT
nduo-2	Reverse	AAGCAGCAAGAGATATACCAGAAT
	Forward	TCAAAAGTGGAGCGGTGCT
nduo-3	Forward	AGAGCGTTTGAATGTGGTTTTGT
	Reverse	AATCCTCCCAAGATGAAGATGAA
nduo-4	Forward	TGCTTATGCTAGCACACGGTT
	Reverse	ACGCCTCCCAGATGTATGAT
nduo-5	Forward	ACCGGTGAGGTCTTTGGTTC
	Reverse	TGTCCTCAAGGCTACCACCT
ctc-1	Forward	GTTATTGCAGTGCCAACAGGT
	Reverse	CAACACCTGTCAACCCACCTA
ctc-2	Forward	TGCTGATGTTATTCATGCTTGGG
	Reverse	TGCTCCACAAATCTCTGAACAT
ctc-3	Forward	CCAGTACACGAGTTGGGAGAG
	Reverse	TGTGATGTGCTCAAGTTACTGT
ctb-1	Forward	GGGATGTTGGTGACATTGCC
	Reverse	TGCTATTAACCTATCGGGCGT
atp-6	Forward	TGCTGCTGTAGCGTGATTAAG
	Reverse	CGCACTGTTAAAGCAAGTGG

Supplementary Table 2. The primers used in biotin-labeled Northern blot

Type	Primer sequences (5'-3')
5S rRNA	5'biotin-ACGGGATGGCGTGCATTCAACGTG
Gly (TCC)	5'biotin-TCAGCATGGATGCCTTCCAAGCATT
iMet (CAT)	5'biotin-TGGGCCCATAACCCAGAGGTCGGTGG
Asp (GTC)	5'biotin-CGCGGATACTCACCACTATACTACCGAGGA
Gln (TGG)	5'biotin-CCTGAGTGCTAACCGCTACACCATGGAACC
Lys (CTT)	5'biotin-GGTGCTCTACCGACTGAGCTAACCGGGC
Ser (AGA)	5'biotin-CAATCTCCTTAACCACTCGGACATGACTGC